First Year *Wilkinson Microwave Anisotropy Probe* (*WMAP*) Observations: On-Orbit Radiometer Characterization

N. Jarosik[1], C. Barnes[1], C. L. Bennett[2], M. Halpern[3], G. Hinshaw[2], A. Kogut[2], M. Limon[2,4], S. S. Meyer[5], L. Page[1], D. N. Spergel[6], G. S. Tucker[7,2,4], J. L. Weiland[8], E. Wollack[2], E. L. Wright[9]

jarosik@pupgg.princeton.edu

ABSTRACT

The *WMAP* satellite has completed one year of measurements of the Cosmic Microwave Background (CMB) radiation using 20 differential high-electron-mobility-transistor (HEMT) based radiometers. All the radiometers are functioning nominally, and characterizations of the on-orbit radiometer performance are presented, with an emphasis on properties that are required for the production of sky maps from the time ordered data. A radiometer gain model, used to smooth and interpolate the CMB dipole gain measurements is also presented. No degradation in the sensitivity of any of the radiometers has been observed during the first year of observations.

Subject headings: cosmology: cosmic microwave background—instrumentation: detectors—space vehicles: instruments

1. INTRODUCTION

The *Wilkinson Microwave Anisotropy Probe* (*WMAP*), launched 2001 June 30, is a Medium-class Explorer (MIDEX) mission designed to produce full sky maps of the cosmic microwave background (CMB)

[1]Dept. of Physics, Jadwin Hall, Princeton, NJ 08544

[2]Code 685, Goddard Space Flight Center, Greenbelt, MD 20771

[3]Dept. of Physics and Astronomy, University of British Columbia, Vancouver, BC Canada V6T 1Z1

[4]National Research Council (NRC) Fellow

[5]Depts. of Astrophysics and Physics, EFI and CfCP, University of Chicago, Chicago, IL 60637

[6]Dept of Astrophysical Sciences, Princeton University, Princeton, NJ 08544

[7]Dept. of Physics, Brown University, Providence, RI 02912

[8]Science Systems and Applications, Inc. (SSAI), 10210 Greenbelt Road, Suite 600 Lanham, Maryland 20706

[9]UCLA Astronomy, PO Box 951562, Los Angeles, CA 90095-1562

[10]*WMAP* is the result of a partnership between Princeton University and NASA's Goddard Space Flight Center. The HEMT amplifiers used in *WMAP* were supplied by the National Radio Astronomy Observatory. Scientific guidance is provided by the *WMAP* Science Team.

radiation. The *WMAP* instrument is comprised of a dual set off-axis Gregorian telescopes (Page et al. 2003b) coupled to 20 differential radiometers (Jarosik et al. 2003). *WMAP* scans the sky from near the second Earth-Sun Lagrange point with a 129 s spin period and a 1 hour precession period (Bennett et al. 2003a). The resulting scan pattern is highly interconnected, minimizing systematic errors in the reconstructed maps. *WMAP* utilizes high electron mobility transistor (HEMT) based amplifiers (Pospieszalski et al. 2000) with cooled input stages to reduce the noise of the radiometers. This paper describes the on-orbit performance of the radiometers with emphasis on those characteristics which determine the quality of the sky maps. Design details and terminology used for the optics, radiometers and overall mission can be found in Page et al. (2003b), Jarosik et al. (2003) and Bennett et al. (2003a) respectively.

Detailed knowledge of the performance of the *WMAP* optics and radiometers is essential in order to convert the raw time ordered data (TOD) into accurate maps of the microwave sky. (Hinshaw et al. 2003) Characterization of both the optics and radiometers employ a combination of pre-launch ground based measurements and on-orbit data. Characterizations of the main beam and sidelobe response of the optics are presented in Page et al. (2003a) and Barnes et al. (2003).

The key radiometer performance parameters are the frequency bandpasses, data collection system responses, and radiometer noise and gain characteristics. The frequency bandpasses and data collection system were fully characterized in pre-launch ground tests and are described in Jarosik et al. (2003). Figure 1 summarizes the audio frequency response of the data collection system together with the frequency roll-offs associated with the beam sizes and the angular spectrum of a typical CMB signal. The radiometer gain and noise properties were also characterized during ground tests, but the final precise measurement of these quantities is done while on orbit since they depend on details of the thermal environment of the radiometers which could not be predicted precisely before launch.

2. THE RADIOMETER THERMAL ENVIRONMENT

Approximately 2 hours after launch, power was applied to the *WMAP* radiometers while the Focal Plane Assembly (FPA) components were at approximately 265 K; all 20 radiometers were observed to be operational. (The FPA comprises the input stages of the radiometers and feed horns and is designed to passively cool to ≈ 90 K.) Over the next 2 days all the major radiometer assemblies, the FPA, the Receiver Box (RXB), the Analog Electronics Unit (AEU) and the Power Distribution Unit (PDU) quickly approached nominal operating temperatures and radiometer performance improved as expected. (See Figure 7 of Bennett et al. (2003a) for an block diagram containing details of these units.) Infrared irradiation from the Earth and Moon during the first month of the mission, the trajectory phasing loops, induced thermal fluctuations in the instrument components, limiting the utility of radiometer performance analyses which could be performed. During this period, however, valuable measurements of beam sidelobe pattern were obtained. These large thermal perturbations ended after the lunar encounter on 2001 July 30, allowing the temperatures of the instrument components to approach their final steady state values. All performance data presented here were taken after 2001 August 10, by which time the satellite temperatures had stabilized and data for the

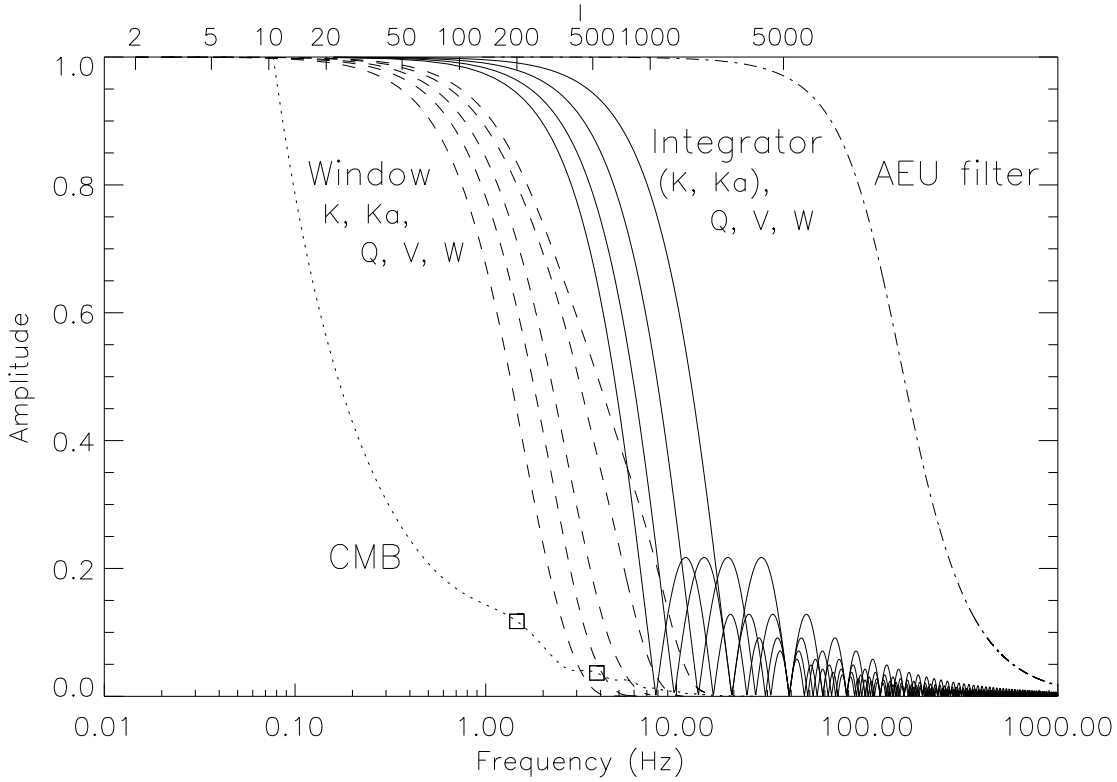

Fig. 1.— Frequency response of the *WMAP* data collection system and some representative input spectra. The curve labeled "AEU filter" (dot-dash) is the amplitude response of the 2-pole Bessel filter ($f_{3\mathrm{dB}}$ = 100 Hz) before the voltage to frequency converter in the Analog Electronics Unit. The 4 solid lines labeled "Integrator" are the absolute values of the sinc functions corresponding to the $128, 102.4, 76.8$ and 51.2 ms integration periods used for the different radiometer frequency bands. (See Figure 8 of Bennett et al. (2003a).) The dashed lines labeled "Window" are the frequency spectra that would result from *WMAP*'s scan pattern and beams if it were observing a scale invariant angular power spectrum ($C_l = const.$) sky based on the window functions in Page et al. (2003a). The dotted line labeled CMB is the input signal to the data collection system which would occur for a typical CMB sky sampled by an ideal pencil beam. The two squares on this last curve show the approximate locations of the first two peaks in the CMB power spectrum. The response of the AEU filter is down from unity by 0.1% at l = 1000, indicating that it has a negligible effect on the shape of the observed power spectra.

first year sky maps were being taken.

WMAP is outfitted with 57 high resolution platinum resistance thermometers that monitor the temperature of representative instrument components. Each thermometer is read out every 23 seconds, has 0.5 mK resolution, ± 1 K accuracy, and ≈ 1 least significant bit of readout noise to allow averaging of multiple samples. There are 17 such thermometers on FPA components, 12 on RXB components, 13 on the optics[11], 9 in the AEU and 6 in the PDU.

Table 1 lists the 12-month mean temperatures, peak-to-peak temperature variations, and limits on the measured spin synchronous temperature variations of the AEU, FPA, PDU and RXB. The total variation also contains a slow annual term arising from the ellipticity of the Earth's orbit modulating the level of insolation on the spacecraft plus a contribution from the initial thermal transient associated with phasing loops and the final lunar encounter. Details of the thermal history of each component are presented in Limon et al. (2003). Future total variations are predicted to be $\approx 1/3-1/2$ the values given in the Table since the transient effects will not be repeated. The spin synchronous term was measured by removing a slowly varying baseline from the temperature data and binning the residual temperature fluctuations synchronously with the spacecraft spin relative to the Sun direction. Keeping the spin synchronous temperature fluctuations at or below the design requirement values is essential in order to meet the systematic error requirements (Jarosik et al. 2003). The measured spin synchronous temperature variations of all the instrument components are at least a factor of *50 smaller* than the maximum allowed values specified in the systematic error budget, the values of which are also presented in Table 1.

3. RADIOMETER PERFORMANCE

3.1. Sensitivity

The radiometers must be calibrated using known input signals to determine their sensitivities. During ground testing at the Goddard Space Flight Center (GSFC), calibrations were performed with thermally regulated full aperture loads attached to the feed horn inputs. On-orbit, the 3 mK CMB dipole signal, coupled into the radiometer through the full optical system, provides a stable calibration signal and is used to track calibration drifts. Absolute calibration is provided by the annual modulation of the dipole signal arising from the known orbital velocity of the Earth about the Sun, and the CMB monopole temperature as determined by Mather et al. (1999). The conversion factors presented in Jarosik et al. (2003) are used to convert the dipole calibrations into Rayleigh-Jeans units.

Table 2 contains the radiometer sensitivities measured at GSFC and on-orbit. The GSFC sensitivities have been scaled to compensate for the difference between the radiometer environments during the ground and on-orbit measurements. The sensitivity values measured during the GSFC test agree fairly well with the values measured on-orbit. The K (23 GHz), Ka (33 GHz), Q (41 GHz), and V (61 GHz) band radiometers

[11]One of the thermometers attached to the top of a radiator panel is non-functional. See Limon et al. (2003) for details.

Table 1. *WMAP* Radiometer Thermal Environment Summary

Assembly	Mean Values (K)	Total Variation (K p-p)	Requirement spin-sync (μK rms)	Measured spin-sync (μK rms)
PDU	295.9 – 298.1	2.64	< 10000	< 7.5
AEU	298.7 – 305.9	2.52	< 10000	< 7.8
RXB	286.4 – 288.5	1.20	< 500	< 7.6
FPA	87.9 – 91.0	0.88	< 500	< 6.4

Note. — This Table summarizes the thermal environment of the *WMAP* radiometers. The ranges specified for the "Mean Values" are 12 month averages of the coldest and hottest thermometer in each assembly. The "Total Variation" values are the largest variations observed for any thermometer within the corresponding assembly. The measured spin synchronous values are obtained by binning measured temperatures in spin synchronous coordinates relative to the Sun, after spline removal of long term temperature drifts. The values presented are derived from one month of data and are the largest limits obtained for any thermometer within each assembly. No significant spin synchronous temperature variations are observed, so the limits presented are determined by the binned readout noise of the thermometers. The measured limits on the spin synchronous temperature variations are at least a factor of 50 smaller than the maximum values allowed by the pre-flight systematic error budget.

seem to have slightly lower noise on-orbit than predicted from the scaled GSFC results. This is thought to be the result of small reflections in the feed horn loads used during the ground test, the effects of which were not included in the analysis. The W (94 GHz) band radiometers appear slightly noisier than predicted. In this case it is thought that the simple power law scaling used to predict the cryogenic HEMT noise temperature based on its physical temperature is inaccurate. Table 2 also contains the estimated mean pixel noise values (3.2×10^{-5} sr/pixel), derived from the measured on-orbit noise levels, for maps created by combining all the radiometer channels in each frequency band for the originally approved 2 year mission and the currently approved extension to a 4 year mission.

3.2. Stability

Ideally the radiometer noise has a flat (white) power spectrum over the audio bandwidth of the signal being measured. Given the *WMAP* beam sizes and scan rates, the signal bandwidth extends from $\approx 0.008-$ 8 Hz. Figure 2 shows a power spectrum of the V12 radiometer noise obtained on-orbit. (See Jarosik et al. (2003) for an explanation of the radiometer labeling conventions.) The noise power spectrum is very flat and only turns up at very low frequencies. The increase in noise at low frequency is characterized by a "1/f knee frequency", $f_{\rm knee}$, taken to be the value at which the noise power spectral density increases to $\sqrt{2}$ times its high frequency value, in this case $f_{\rm knee}$ = 1.12 mHz. Table 2 contains the values of $f_{\rm knee}$ measure on-orbit for all the radiometers. Most of the radiometers have $f_{\rm knee}$ values below 8 mHz, the low frequency end of the signal bandwidth, but a few are problematic, particularly W41 and W42.

The radiometer offset temperatures, $T_{\rm off}$, measured at GSFC and on-orbit are also presented in Table 2. These values correspond to the size of the radiometer output signal when both inputs are observing regions with the same antenna temperatures. (See Jarosik et al. (2003) for the precise definition of $T_{\rm off}$ used for *WMAP*.) A significant correlation between the magnitude of the radiometer offset, $T_{\rm off}$, and value of $f_{\rm knee}$ is expected for differential radiometers; this correlation arises from radiometer gain fluctuations modulating the radiometer offset signal. If it is assumed that all the amplification chains in the radiometers have power gain fluctuations of the same fractional amplitude and frequency spectra proportional to $f^{-\alpha}$, then the $f_{\rm knee}$ is expected to scale as $f_{\rm knee} \propto (|T_{\rm off}|\Delta\nu^{1/2}/T_{\rm sys})^{2/\alpha}$. Here $T_{\rm sys}$ and $\Delta\nu$ are the radiometer system noise temperatures and noise equivalent bandwidths. Figure 3 shows on-orbit data for the 20 *WMAP* radiometers. The value of the exponent α measured from these data is 1.70, somewhat larger that the value of 0.96 reported by Wollack & Pospieszalski (1998). Direct comparison of these values of α is complicated by the fact that the data contained in Figure 3 comes from 20 different radiometers fabricated from HEMT devices with three different geometries, while the Wollack & Pospieszalski (1998) results were obtained from measurements on a single amplification chain. The difference between the measured values of α may therefore not be significant.

The source of the high value of $f_{\rm knee}$ in the W41 and W42 radiometers is the large $|T_{\rm off}|$ for these radiometers. The on-orbit values of $|T_{\rm off}|$ are significantly larger than the values measured during the GSFC tests for the W21, W22, W41 and W42 radiometers. The fact that the radiometer $f_{\rm knee}$ values track the

Table 2. Radiometer Performance Summary

Radiometer	Sensitivity (mK $\sec^{1/2}$)		ΔT/pixel (μK)	$f_{\rm knee}$ (mHz)		$T_{\rm off}$ (K)		$\Delta T_{\rm ss}$ (μK rms)
	GSFC	Flight	4 yr (2 yr)	GSFC	Flight	GSFC	Flight	Flight
K11	0.72	0.66	19.4 (27.5)	6.13	0.40	-0.033	0.19	< 0.02
K12	0.87	0.75		5.37	0.51	-0.249	0.22	< 0.02
Ka11	0.75	0.71	19.9 (28.2)	1.66	0.71	0.387	0.49	< 0.03
Ka12	0.77	0.72		1.29	0.32	0.072	0.25	< 0.02
Q11	0.99	0.92	20.5 (29.0)	3.21	1.09	0.092	–0.11	< 0.04
Q12	0.95	1.02		3.13	0.35	0.142	0.12	< 0.02
Q21	0.89	0.85		1.92	5.76	0.552	1.14	< 0.03
Q22	1.04	0.99		4.61	8.62	1.036	1.54	< 0.15
V11	1.25	1.22	24.0 (34.0)	2.56	0.09	-0.448	0.06	< 0.01
V12	1.07	1.11		4.49	1.41	-0.270	0.24	< 0.04
V21	1.01	0.97		2.43	0.88	-0.265	0.31	< 0.04
V22	1.13	1.10		3.06	8.35	0.352	0.95	< 0.01
W11	1.18	1.35	23.1 (32.7)	16.17	7.88	-0.451	1.40	< 0.01
W12	1.41	1.61		15.05	0.66	-2.064	–0.10	< 0.09
W21	1.38	1.61		1.76	9.02	-0.091	1.41	< 0.02
W22	1.44	1.72		0.77	7.47	0.008	1.53	< 0.01
W31	1.47	1.65		1.84	0.93	-1.151	–0.39	< 0.04
W32	1.69	1.86		2.39	0.28	-1.117	0.05	< 0.17
W41	1.60	1.71		8.46	46.5	1.300	3.33	< 0.02
W42	1.43	1.65		5.31	26.0	1.441	3.27	< 0.12

Note. — Summary of the sensitivities, $f_{\rm knee}$, $T_{\rm off}$, of the 20 radiometers comprising *WMAP* as measured during integration and testing (GSFC) and on-orbit at Earth-Sun L2. The sensitivity values given are for the combined output of the two detectors on each radiometer, e.g. K113 + K114. The values of ΔT/pixel are for all radiometers in each frequency band combined. The sensitivity values from ground tests have been scaled to approximate those expected on-orbit for an FPA temperature of 89 K. The pixel noise estimate assumes 4 (2) years of data, 3.2×10^{-5} sr/pixel, and uniform sky coverage. The last column contains limits on spin synchronous artifacts in the time ordered data, $\Delta T_{\rm ss}$, obtained from combining the products of the temperature susceptibility coefficients measured during grounds tests with the spin synchronous temperature fluctuation limits from Table 1. These data indicate that the radiometers are functioning properly and that spin synchronous artifacts in the time ordered data are expected to be much smaller that the maximum values permitted (2.8 μK) in the systematic error budget. All temperatures are in Rayleigh-Jeans units.

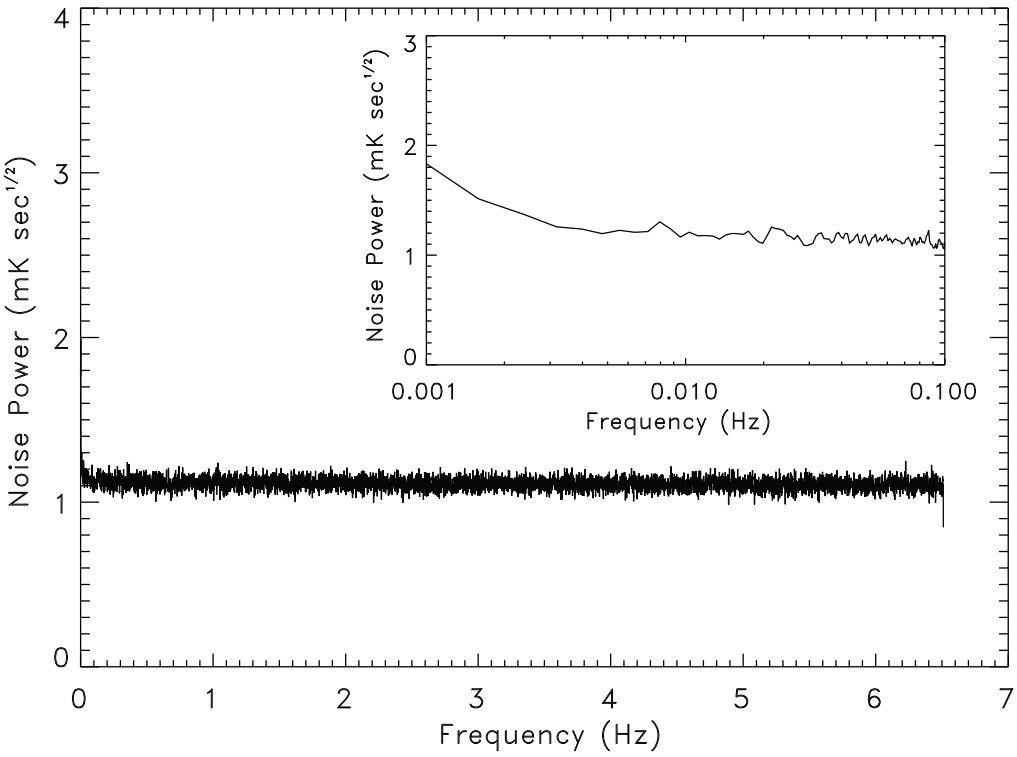

Fig. 2.— Noise power spectral density of the V12 radiometer obtained from 3 days of on-orbit data. Sky signals arising from the dipole, CMB, Galaxy and point sources have been removed. The inset contains an expanded view of the low frequency region of the same data. The flat spectrum down to very low frequencies ($f_{\rm knee}$ = 1.41 mHz) indicates proper radiometer performance.

measured values of $|T_{\rm off}|$, as shown in Figure 3, indicates the radiometers are operating as expected. The exact source of the larger $|T_{\rm off}|$ values is not known.

Even with the relatively low values of $f_{\rm knee}$ for the majority of the radiometers, noise correlations are not negligible. Maps produced directly from radiometer data for radiometers with $f_{\rm knee} \lesssim f_{\rm spin} = 7.75$ mHz exhibited small but detectable pixel noise correlations ("stripes") which could corrupt power spectrum determinations. In order to minimize these effects in the final sky maps, a pre-whitening procedure has been adopted which fits a baseline to the TOD after removal of an estimated sky signal obtained from the sky maps. Details of the pre-whitening process are presented in Hinshaw et al. (2003).

The last column in Table 2 presents limits to spin synchronous artifacts in the TOD for each of the radiometers. These values were determined by multiplying the limits on the spin synchronous temperature fluctuations of each radiometer section (AEU, PDU, FPA and RXB) by the appropriate susceptibility coefficient determined during ground testing, and summing values in quadrature. Hinshaw et al. (2003) obtain similar results using susceptibility coefficients derived from on-orbit data. In all cases the limits on spin synchronous artifacts are much smaller than the 2.8 μK allocated to the radiometers and data collection system in the systematic error budget (Jarosik et al. 2003).

It is possible to obtain an estimate of spin synchronous artifacts directly from the TOD independent of any model of its source. This was accomplished by binning 40 days of TOD (after removal of the CMB dipole signal) in an azimuthal coordinate about the spin axis of the spacecraft. (Recall the Sun's elevation is fixed during observations by the *WMAP* scan pattern.) Each TOD point was binned according to the Sun's location at the time of the observation, and bin averages calculated. TOD from all of the V and W band radiometers was used and a 10° Galactic cut applied. The limit obtained by this technique is $\Delta T_{\rm ss} < 0.14$ μK rms, well below the 9 μK value allowed in the systematic error budget (Jarosik et al. 2003). Note that this limit includes any artifacts which originate in the radiometers, data collection system or optical system. Since both the estimated and measured systematic error limits are so small, *no corrections arising from spin synchronous radiometric artifacts are applied to the TOD in the production of the one year sky maps.*

During the data period incorporated in the 1 year maps a total of 21 sudden jumps ("glitches") have occurred in the outputs of the radiometers. Jumps were exhibited by the Ka11, Ka12, Q11, Q12 and W12 radiometers. Of these events, 19 involved single radiometers, one simultaneously affected two radiometers and one affected three. Similar artifacts were observed during ground testing and have been identified as small parameter shifts in the properties of several microwave components resulting from sudden releases of internal mechanical stresses. The most common events involve the phase switches and filters, which are constructed with suspended stripline elements, but events have also been observed involving waveguide components connecting the orthomode transducers to the inputs of the radiometers. These events result in a negligible change in radiometer performance, but must be identified and excised from the TOD in production of the maps. Although the duration of each event is short, < 1 s, the data processing pipeline (Hinshaw et al. 2003) requires removal of several hours of data surrounding each event resulting in a data loss of $\approx 0.13\%$. A complete tabulation of these events can be found in Limon et al. (2003).

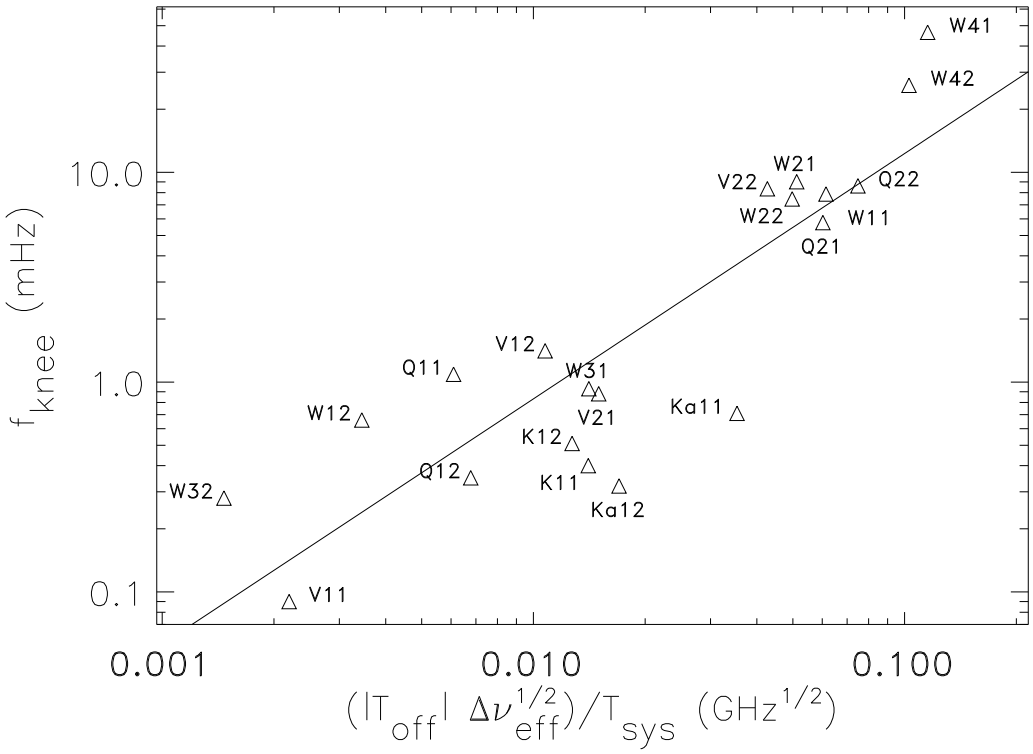

Fig. 3.— Dependence of $f_{\rm knee}$ on $T_{\rm off}$ for the 20 radiometers comprising *WMAP*. The solid line is a power law fit to the data of the form $f_{\rm knee} \propto ((|T_{\rm off}|\Delta\nu_{\rm eff}^{1/2})/T_{\rm sys})^{2/\alpha}$ with $\alpha = 1.70$. The scaling of $f_{\rm knee}$ with $T_{\rm off}$ indicates that $f_{\rm knee}$ is largely determined by radiometer gain fluctuations modulating the signal from the radiometer offsets, as expected.

3.3. Input Transmission Imbalance

Ideally the output of each *WMAP* radiometer would exhibit a purely differential response to sky signals, rejecting any common mode component. This is not true if the power transmission coefficients, $\alpha_{\rm A}$ and $\alpha_{\rm B}$, of the optics and waveguide components, which couple the sky signals from the A and B side beams to the radiometer, are not equal. In this case the output of a radiometer, S, when the beams observe regions of sky with antenna temperatures T_A and T_B will be

$$S = G(\alpha_{\rm A} T_A - \alpha_{\rm B} T_B), \tag{1}$$

where G is the gain of the radiometer.

Using the CMB dipole signal it is possible to measure the common mode response of a radiometer to sky signals and therefore infer the value of $\alpha_{\rm A} - \alpha_{\rm B}$. Figure 4 shows the pure predicted differential and common mode CMB dipole signals, $T_d = T_A - T_B$ and $T_c = T_A + T_B$, for a typical 2 hour period of *WMAP* observations. Note that T_d and T_c are very nearly orthogonal when averaged over a precession period due to the symmetry of *WMAP*'s scan pattern. (Bennett et al. 2003a) The common mode signal is comprised of three terms. The first appears as the −1.8 mK offset in the figure and is modulated on the one year timescale as *WMAP*'s precession axis changes orientation with respect to the CMB dipole axis. This signal component is at such a low frequency and amplitude that it cannot be distinguished from long term drifts in the radiometer offsets. The other two terms vary on the timescale of the precession (1 h) and the spin (129 s), with most of the power being in the lower frequency component. The amplitude of these two signals combined is ≈ 0.5 mK, so a 1% common mode response corresponds to a signal amplitude of $\approx 5\ \mu$K.

The common mode radiometric response was measured by fitting the raw radiometer TOD to a function of the form

$$S(t_j) = \sum_{\rm i=0}^{3} c_i (t_j - t_0)^i + \beta_c T_c(t_j) + \beta_d T_d(t_j), \tag{2}$$

where t_j is the time of the observations, c_i are polynomial coefficients used to remove a baseline, T_c and T_d are the common mode and differential CMB dipole signal templates and β_C and β_S are the coefficients to be fit. Raw data must be used since the calibration and baseline fitting procedures (Hinshaw et al. 2003) remove most of the very low frequency (≈ 0.3 mHz) signal we are attempting to measure. The measured values of β_c and β_d are related to the transmission coefficients $\alpha_{\rm A}$ and $\alpha_{\rm B}$ by

$$\beta_c = \frac{G}{2}(\alpha_{\rm A} - \alpha_{\rm B}) \tag{3}$$

$$\beta_d = \frac{G}{2}(\alpha_{\rm A} + \alpha_{\rm B}). \tag{4}$$

The TOD is divided into segments containing an integral number of precession periods, $n_{\rm prec}$, and a function of the form given by Equation 2 fit to each segment. Observations at Galactic latitude $|b| < b_{\rm min}$ are excluded from the fits. Values of the fractional transmission imbalance, $x_{\rm im}$, defined as

$$x_{\rm im} \equiv \frac{\langle \beta_c \rangle}{\langle \beta_d \rangle} = \frac{\langle \alpha_{\rm A} - \alpha_{\rm B} \rangle}{\langle \alpha_{\rm A} + \alpha_{\rm B} \rangle} \approx \frac{\alpha_{\rm A} - \alpha_{\rm B}}{2}, \tag{5}$$

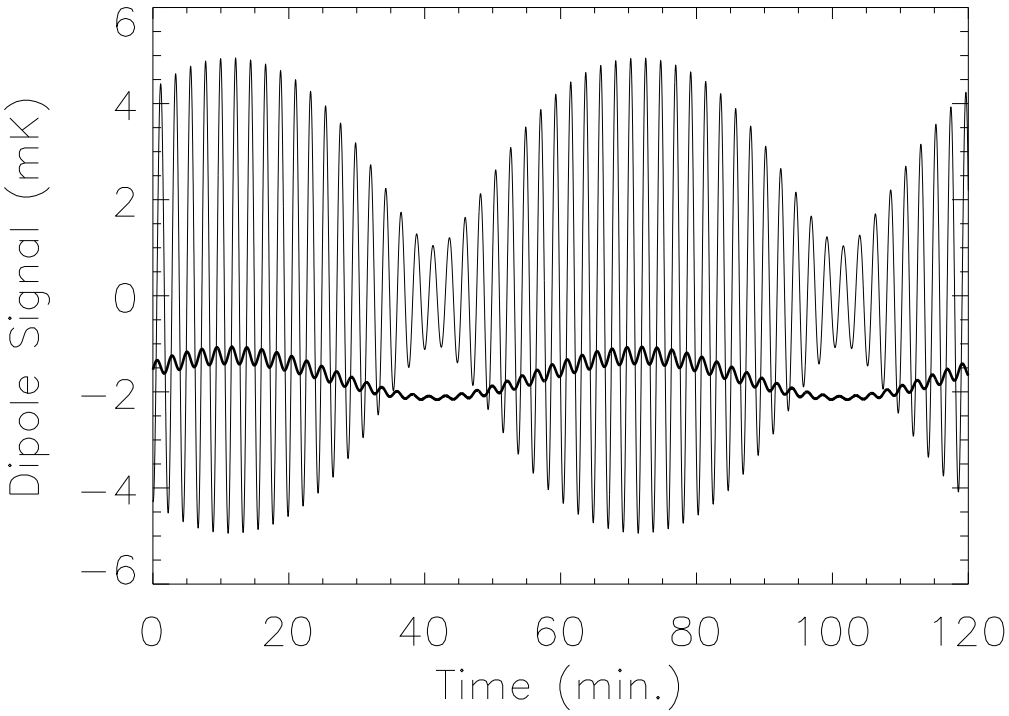

Fig. 4.— Predicted differential (thin) and common mode (thick) CMB dipole signal for a typical 2 hour period of *WMAP* observations. The rapid period ($\approx$ 2 minute) corresponds to *WMAP*'s spin rate and the slower period (1 hr) to the precession rate. Measurement of the common mode signal component in a radiometer's output allows characterization of the non-ideal (common mode) radiometric response.

are presented in Table 3. The braces indicate a weighted average of the measured coefficients, β_c and β_d, over the 232 day period used in the analysis. The results of the fits are insensitive to the values of $n_{\rm prec}$ chosen in the range of 4-10, indicating that the baseline removal polynomial is not removing a significant amount of common mode signal. The fit values are also insensitive to the value of $b_{\rm min}$ used provided $b_{\rm min} > 10°$, indicating that Galactic signals are not biasing the results.

A differential loss in the input waveguides and optics should also contribute to radiometric offsets, since the lossy components will also emit radiation. The contribution to the radiometer offsets arising from such a differential loss can be estimated as

$$\Delta T_{\rm off} = [(\alpha_{\rm A} T_{\rm CMB} + (1-\alpha_{\rm A}) T_{\rm FPA}) - (\alpha_{\rm B} T_{\rm CMB} + (1-\alpha_{\rm B}) T_{\rm FPA}) \quad (6)$$

$$= (\alpha_{\rm A} - \alpha_{\rm B})(T_{\rm CMB} - T_{\rm FPA}) \quad (7)$$

$$\simeq 2 x_{\rm im} (T_{\rm CMB} - T_{\rm FPA}), \quad (8)$$

where it has been assumed that all the loss occurs at physical temperature $T_{\rm FPA}$ and $\alpha_{\rm A} \simeq \alpha_{\rm B} \simeq 1$. This effect is expected to have a significant contribution to the total $T_{\rm off}$ of each radiometer. Figure 5 displays the values of $T_{\rm off}$ measured in flight and those predicted from Equation 8, assuming $T_{\rm FPA} - T_{\rm CMB}$ = 86 K. A significant correlation is evident between the values predicted by this model and the observed values, supporting the validity of the technique.

The model of the radiometer response to sky signals used in the map making procedure (Hinshaw et al. 2003) is

$$S = G \left[\frac{\alpha_{\rm A} - \alpha_{\rm B}}{2} T_{\rm c} + \frac{\alpha_{\rm A} + \alpha_{\rm B}}{2} T_{\rm d} \right] \quad (9)$$

$$S = G' [(1 + x_{\rm im}) T_{\rm A} - (1 - x_{\rm im}) T_{\rm B}], \quad (10)$$

where the mean of the input transmission coefficients, $(\alpha_{\rm A} + \alpha_{\rm B})/2$, has been absorbed in the measured gain, G', determined by fitting the differential CMB dipole signal.

3.4. Noise Statistics

The intrinsic radiometer noise is expected to exhibit a Gaussian distribution. A plot of the V12 radiometer noise distribution obtained from 10 days of data is presented in Figure 6. This data period was chosen to be free of disturbances (such as orbital station keeping maneuvers) and its duration short enough so that the slow variations in system noise, driven by the annual temperature variation of the FPA, could be ignored. The noise signal was obtained by removing the CMB dipole and an estimated sky signal (obtained from the final maps) from the pre-whitened TOD. Data when either of the beams was in a region of high Galactic emission (as determined by the Kp4 mask (Bennett et al. 2003b)) or near a planet were cut. No other cuts were made. The distributions for all 20 radiometers exhibited similar behavior, following Gaussian distributions over at least 5 decades. No statistically significant skewness or kurtosis is observed in the noise distributions of any of the radiometers.

Table 3. Input Transmission Imbalance Measurements of the *WMAP* Radiometers

Radiometer	$x_{\rm im}$	Radiometer	$x_{\rm im}$
K11	-0.00204	K12	-0.00542
Ka11	0.00115	Ka12	0.00108
Q11	-0.00200	Q12	0.00010
Q21	0.01251	Q22	0.01433
V11	-0.00354	V12	-0.00015
V21	0.00682	V22	0.00598
W11	0.00846	W12	0.00581
W21	0.01550	W22	0.00849
W31	0.00253	W32	0.00542
W41	0.01536	W42	0.01581

Note. — Measurement of the fractional input transmission imbalance, $x_{\rm im}$, obtained from 232 days of data with $n_{\rm prec} = 10$ and $b_{\rm min} = 15^\circ$. They were obtained via measurements of the radiometer responses to the common mode signal arising from the CMB dipole. All the values are small, nevertheless corrections for this effect have been included in the map making algorithm.

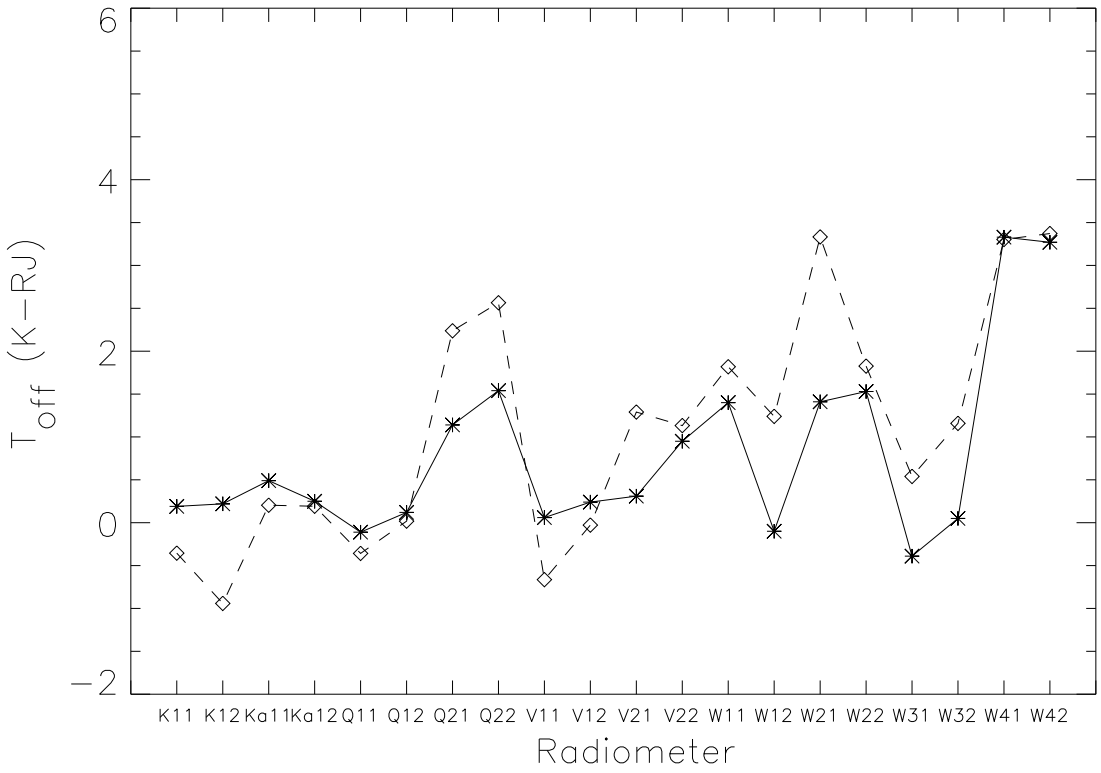

Fig. 5.— On-orbit measurements of the radiometer offset temperatures, $T_{\rm off}$ (stars), and predicted contributions to the offset temperature, $\Delta T_{\rm off}$ (diamonds), for all 20 *WMAP* radiometers. Values of $\Delta T_{\rm off}$ are obtained from measurements of the radiometer common mode responses to the CMB dipole signal. Significant correlation between the measured offset and the predicted values of $\Delta T_{\rm off}$ are expected and observed. The lines are drawn to aid in seeing the correlation.

Given the Gaussian noise distribution, the noise variance in a given pixel of the final sky maps should scale inversely with the number of observations of each pixel, $N_{\rm obs}$. This is tested by measuring the variance of each set of map pixels with a given value of $N_{\rm obs}$ and plotting it against $N_{\rm obs}^{-1}$, as in Figure 7. Pixels with large Galactic signals and point sources have been excluded based on the Kp4 mask. (The values of $N_{\rm obs}$ have been corrected to account for small variations in the radiometer noise levels resulting from changes in the radiometers physical temperatures. Values of $N_{\rm obs}$ are therefore not integers, but are scaled to correspond to a mean noise value.) Since the CMB fluctuations are uncorrelated with the instrument noise, they add a constant variance to each bin. The slope of the line fit to the data is a measure of the noise per observation, while the y-intercept is the variance arising from the CMB fluctuations. The noise variance clearly scales as predicted, indicating that $N_{\rm obs}^{-1}$ is a good predictor of the pixel noise.

4. RADIOMETER GAIN MODEL

The primary gain calibration of *WMAP* is derived from observations of the CMB dipole. Although quite stable, small changes in the radiometer thermal environment produce measurable changes in the radiometer gains. Gain measurements with errors of $\approx 1\%$ are obtained from each hour of observations. A gain model, relating instrument housekeeping data to the observed radiometric gain, has been developed to aid in smoothing and interpolating the hourly gain measurements. This model also reduces the uncertainty in gain determination when the dipole derived gain measurements degrade as a result adverse alignment of the scan pattern with the dipole orientation or the Galactic plane.

Following the notation of Jarosik et al. (2003), the modulated microwave power incident on a detector, $v_{\rm in}^2$, arising from an antenna temperature difference, $\Delta T = (A^2 - B^2)$, may be written as

$$v_{\rm in}^2 = \frac{1}{2}(A^2 - B^2) g_1 g_2 \cos(\theta). \tag{11}$$

where g_1 and g_2 are the voltage gains of the two amplification chains in the radiometer and $\cos(\theta)$ is a term that accounts for phase mismatches in the radiometer.

The output voltage from the detector with input power $v_{\rm in}^2$ is described by a response function $s(v_{\rm in}^2)$. (This treatment differs from that given in Jarosik et al. (2003) in that the response of the detector to the input power is described by a non-linear response function, $s(v_{\rm in}^2)$, to allow for deviations from square law response and gain compression which can occur in the warm HEMT amplifiers.) For the small ($< 2\%$) changes in detector input power it suffices to linearize this response about the nominal operating point,

$$s(v_{\rm in}^2) = V_0 + \tilde{s} v_{\rm in}^2. \tag{12}$$

where $\tilde{s}$ is the differential responsivity of the detector and V_0 is a parameter to be fit. The *modulated* voltage output from the detector is then

$$S = \tilde{s}(v_{\rm in}^2) = \frac{\tilde{s}}{2}(A^2 - B^2) g_1 g_2 \cos(\theta). \tag{13}$$

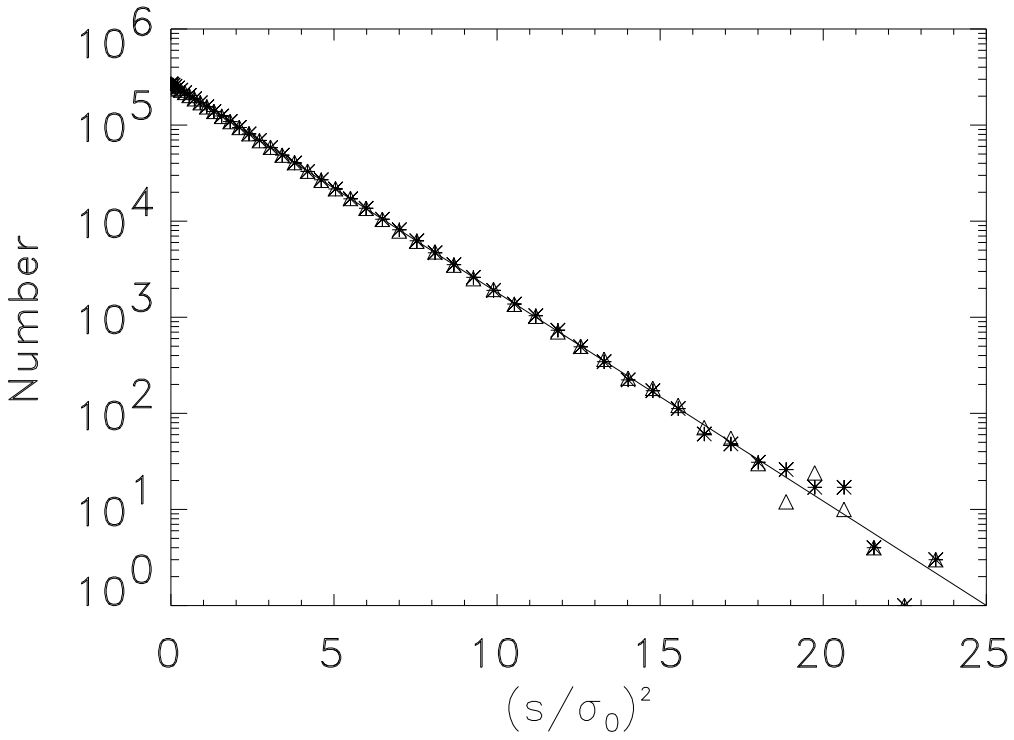

Fig. 6.— Distribution of the pre-whitened V12 radiometer noise obtained from ten days of observations. Sky signals arising from the dipole, CMB and Galaxy have been removed. Data points were cut when either radiometer beam encountered a planet or a region of high Galactic emission. The line corresponds to a unit variance Gaussian distribution normalized to the observed frequency at $s = 0$. The two symbols denote the values obtained from the two sides of the distribution. The highly Gaussian distribution indicates that the noise variance for each pixel of the resulting sky maps should scale inversely with the number of observations of that pixel.

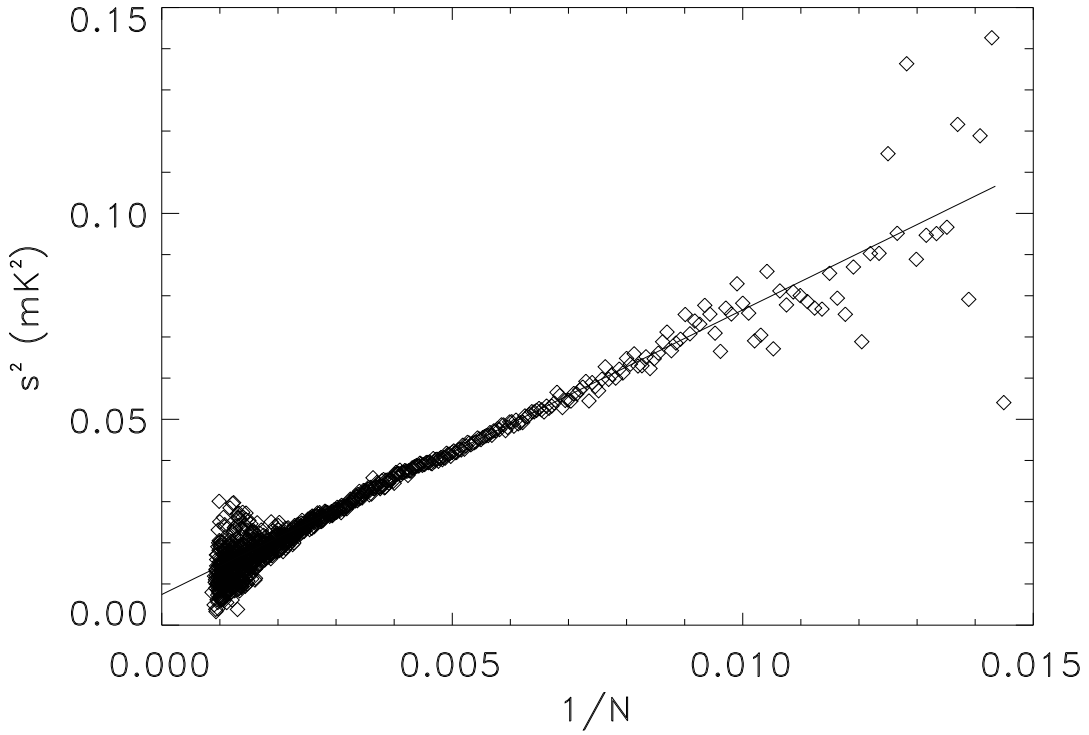

Fig. 7.— Measured sample variance, s^2, dependence on normalized number of observations, $N_{\rm obs}$, for the V1 sky map. The diamonds are the sample variances measured from each subset of map elements for which $N-0.5 < N_{\rm obs} < N+0.5$. The solid line is a linear fit to the data. As expected, the noise variance scales as $N_{\rm obs}^{-1}$, confirming that it is a good predictor of the pixel noise.

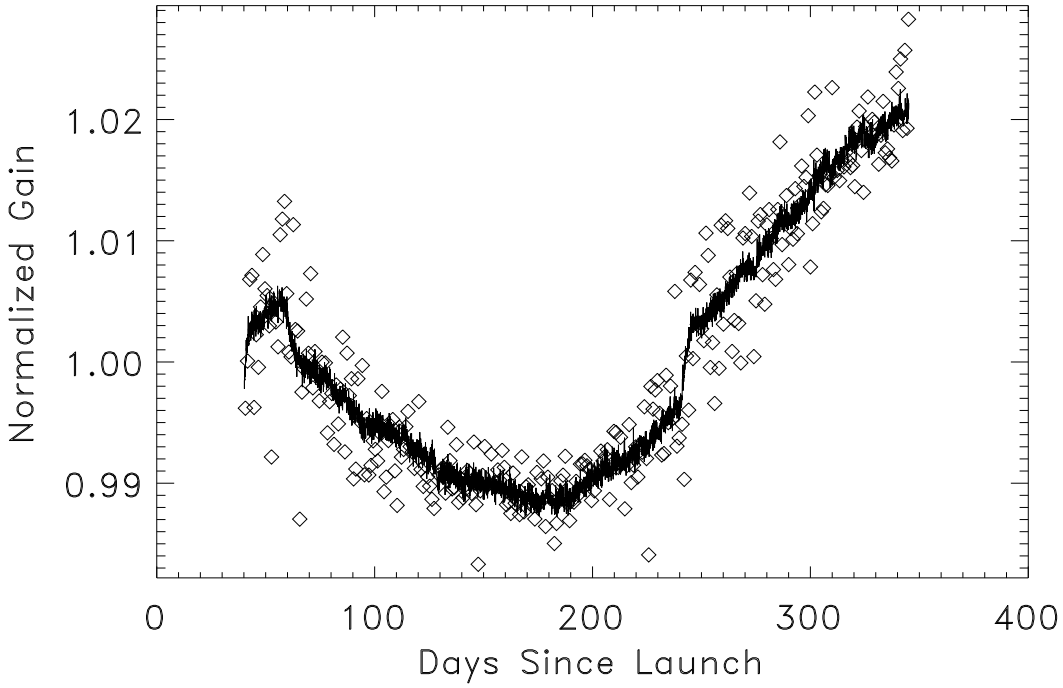

Fig. 8.— Comparison of the V11 radiometer gains measured from the CMB dipole (diamonds) and the gain model (solid line). The CMB derived gains are 24 hour averages. The high frequency noise in the gain model arises from the quantization of the RF bias housekeeping data. The rapid gain change ≈ 245 days after launch is the result of a small (0.5 K) change of the RXB temperature as a consequence of an adjustment of the spacecraft's main bus voltage. Note the entire vertical scale spans a $\approx 4\%$ range. The model clearly tracks the measured gain values well and is therefore useful in smoothing and interpolating the hourly gain measurements.

The DC (unmodulated) power out of the same detector, $\overline{V}$, is given by

$$\overline{V} = V_0 + \frac{\tilde{s}}{2}\left\{\left(\frac{A^2+B^2}{2}+n_1^2\right)g_1^2 + \left(\frac{A^2+B^2}{2}+n_2^2\right)g_2^2\right\} \tag{14}$$

where n_1 and n_2 are the instantaneous noise voltages added by the HEMT amplifiers and the overbar indicates an average on time scales long compared to the period of the microwave signal. The idea is to use the values of $\overline{V}$, measured to $\approx 0.1\%$ every 23.6 s, to estimate the value of $g_1 g_2$, which, according to equation 13, determines the signal gain of the radiometer. Using the approximation

$$\frac{(A^2+B^2)}{2}+n_1^2 \approx \frac{(A^2+B^2)}{2}+n_2^2 \approx n_0^2 \tag{15}$$

Equation 14 can be rewritten as

$$\frac{\overline{V}-V_0}{n_0^2} = \tilde{s}\,\frac{\overline{g_1^2}+\overline{g_2^2}}{2} \approx \tilde{s}\overline{g_1 g_2} \tag{16}$$

provided that

$$\frac{|g_1-g_2|}{|g_1+g_2|} \ll 1. \tag{17}$$

The term n_0^2 corresponds to the average system noise temperature, which is dominated by the input voltage noise of the cryogenic HEMT amplifiers and as such is a slowly varying function of the physical temperature of the HEMT amplifiers, $T_{\rm FPA}$. Again, since the fractional temperature variations are small, it suffices to describe small changes in noise temperature using the relation

$$n_0^2(T_{\rm FPA}) = \alpha^{-1}(T_{\rm FPA}-T_0). \tag{18}$$

Combining equations 13, 16, and 18 yields

$$S = \alpha\frac{\overline{V}-V_0}{T_{\rm FPA}-T_0}(A^2-B^2). \tag{19}$$

Using measured values of the radiometer response, S, $T_{\rm FPA}$, and $\overline{V}$, and the known differential dipole signal, A^2-B^2, it is possible to determine the parameters V_0, T_0 and α. Once these parameters are determined the radiometer gain can be estimated using the measured values of $T_{\rm FPA}$ and $\overline{V}$. Figure 8 shows the gain measured daily using the CMB dipole, and the result from fitting the gain model for the V11 radiometer. The model clearly tracks the dipole derived gain measurements well, and has substantially less scatter. Values of the gain model parameters for all the detectors are presented in Limon et al. (2003).

Since the gain model depends only on the measured RF bias and temperature of the FPA amplifiers, the fact that it fits the measured dipole gains well over such a long period (1 year for this data set) indicates that radiometer characteristics are stable. Had some secular degradation occurred, for example a slowly increasing amplifier noise temperature or phase mismatch, constant values of the fit parameters, α, T_0 and V_0 would not provide a good fit to the measured values for the entire time period. Based on the accuracy of the fits there is no significant degradation in performance of any of the radiometer channels at the 1% level.

5. SUMMARY

All 20 differential radiometers aboard the *WMAP* satellite are functional with close to nominal performance. On-orbit values of the radiometer offset temperatures are slightly higher than expected, leading to higher than expected $1/f$ knee frequencies in two of the radiometers. Spin synchronous systematic errors from the radiometers and data collections system are expected to be < 0.17 μK for all radiometers, and the radiometer noise distributions for all channels are well described by Gaussians. A gain model based on instrument housekeeping data has been developed to aid in interpolating and smoothing the hourly gain calibrations derived from the CMB dipole signal. No significant degradation in radiometer performance has been observed during the first year of observations.

The *WMAP* mission is made possible by the support of the Office of Space Sciences at NASA Headquarters and the efforts of numerous scientists, engineers, machinists, managers, and office and administrative staffs at participating institutions.

REFERENCES

Barnes, C. et al. 2003, ApJ, submitted

Bennett, C. L., Bay, M., Halpern, M., Hinshaw, G., Jackson, C., Jarosik, N., Kogut, A., Limon, M., Meyer, S. S., Page, L., Spergel, D. N., Tucker, G. S., Wilkinson, D. T., Wollack, E., & Wright, E. L. 2003a, ApJ, 583, 1

Bennett, C. L., Halpern, M., Hinshaw, G., Jarosik, N., Kogut, A., Limon, M., Meyer, S. S., Page, L., Spergel, D. N., Tucker, G. S., Wollack, E., Wright, E. L., Barnes, C., Greason, M., Hill, R., Komatsu, E., Nolta, M., Odegard, N., Peiris, H., Verde, L., & Weiland, J. 2003b, ApJ, submitted

Hinshaw, G. F. et al. 2003, ApJ, submitted

Jarosik, N. et al. 2003, ApJS, 145

Limon, M., Wollack, E., Bennett, C. L., Halpern, M., Hinshaw, G., Jarosik, N., Kogut, A., Meyer, S. S., Page, L., Spergel, D. N., Tucker, G. S., Wright, E. L., Barnes, C., Greason, M., Hill, R., Komatsu, E., Nolta, M., Odegard, N., Peiris, H., Verde, L., & Weiland, J. 2003, unknown

Mather, J. C., Fixsen, D. J., Shafer, R. A., Mosier, C., & Wilkinson, D. T. 1999, ApJ, 512, 511

Page, L. et al. 2003a, ApJ, submitted

—. 2003b, ApJ, 585, 0

Pospieszalski, M. W., Wollack, E. J., Bailey, N., Thacker, D., Webber, J., Nguyen, L. D., Le, M., & Lui, M. 2000, in IEEE MTT-S International Microwave Symposium Digest, ed. V. 1 No. Vol. 1, Boston, MA, 25 – 28

Wollack, E. J. & Pospieszalski, M. W. 1998, IEEE MTT-S International Microwave Symposium Digest, 669